Critical look at cosmological perturbation theory techniques

Jordan Carlson[*]

Department of Physics, 366 LeConte Hall, University of California, Berkeley, California 94720, USA

Martin White[†]

Departments of Physics and Astronomy, 601 Campbell Hall, University of California, Berkeley, California 94720, USA

Nikhil Padmanabhan[‡]

Physics Division, Lawrence Berkeley National Laboratory, 1 Cyclotron Road, Berkeley, California 94720, USA

Recently, a number of analytic prescriptions for computing the nonlinear matter power spectrum have appeared in the literature. These typically involve resummation or closure prescriptions which do not have a rigorous error control, thus they must be compared with numerical simulations to assess their range of validity. We present a direct side-by-side comparison of several of these analytic approaches, using a suite of high-resolution N-body simulations as a reference, and discuss some general trends. All of the analytic results correctly predict the behavior of the power spectrum at the onset of nonlinearity, and improve upon a pure linear theory description at very large scales. All of these theories fail at sufficiently small scales. At low redshift the dynamic range in scale where perturbation theory is both relevant and reliable can be quite small. We also compute for the first time the two-loop contribution to standard perturbation theory for cold dark matter models, finding improved agreement with simulations at large redshift. At low redshifts however the two-loop term is larger than the one-loop term on quasilinear scales, indicating a breakdown of the perturbation expansion. Finally, we comment on possible implications of our results for future studies. A software package implementing the methods presented here is available at http://mwhite.berkeley.edu/Copter.

I. INTRODUCTION

The character and evolution of the large-scale structure of the Universe has been the subject of much research in recent decades. As it is currently understood, the large-scale structure grows through a process of gravitational instability starting from a nearly scale-invariant spectrum of Gaussian fluctuations at early times. On very large scales the matter distribution of our universe today is well modeled by linear perturbation theory. On scales below about 10 Mpc, on the other hand, the dynamics are highly nonlinear and we must resort to direct numerical simulations of the N-body problem to understand the clustering of matter or its tracers.

On intermediate, or quasilinear, scales there is the possibility that the matter distribution may be modeled analytically by extending perturbation theory beyond linear order. This possibility has received renewed attention recently due to the interest in using baryon acoustic oscillations (BAO) as a probe of the expansion history of the Universe and of the nature of dark energy [1]. Since the baryonic features are at large scales ($\mathcal{O}(100)$ Mpc) it is plausible that higher-order perturbation theory could model subtle corrections to the linear result with some

accuracy. More generally, investigation of perturbation theory may allow some improvement in theoretical predictions for the next generation of very large surveys.

Consequently, a number of new ideas have been introduced in recent years for computing statistical properties of the matter distribution, most importantly the two-point function or power spectrum. Regrettably these approaches involve uncontrolled approximations, providing no simple way of estimating the theoretical uncertainty. Since perturbation theory is expected to fail on sufficiently small scales, the domain of validity of any particular approach is therefore unclear, and the only known way to test their accuracy is to compare their predictions with the results of N-body simulations. In the past this has been done on a case-by-case basis, with one theory tested for one cosmology against one suite of N-body simulations, focusing primarily on the power spectrum. Recently there have been some attempts to compare multiple theories simultaneously [2,3], or to examine statistics other than the power spectrum [4–6]. However, a comprehensive comparison has been lacking, and with the recent proliferation of analytic techniques it is natural to ask how well these theories actually perform. With near-future observations potentially depending on these techniques and with recent advances in N-body algorithms and computing power, it is timely to revisit this issue.

In this paper we present a direct comparison of several recent analytic predictions for the clustering of matter on

[*]jwgcarlson@berkeley.edu
[†]mwhite@berkeley.edu
[‡]NPadmanabhan@lbl.gov

quasilinear scales. We restrict our attention to the matter fluctuations, because very few of the existing treatments can handle biased tracers such as dark matter halos and galaxies. We use modern, high-resolution N-body simulations as our reference points, which provide highly accurate [7–9] (though computationally expensive) estimates for statistical observables of the matter distribution. By comparing the analytic predictions for two cosmologies, one close to the current best-fit model and one more extreme, we are able to judge the relative merits of each approach.

The paper is organized as follows. In Sec. II we start by reviewing the dynamical equations that govern the evolution of the matter distribution and discuss the relevant statistical quantities that one may compute. We then continue by summarizing the different analytic approaches we consider in this paper. In Sec. III we describe the N-body simulations that are used as a reference point for the comparison. In Sec. IV we plot the various approaches together, discuss qualitatively how well they agree with

simulations, and propose several ways to quantify this agreement. We discuss the results of this comparison in Sec. V, and make some closing remarks in Sec. VI.

II. ANALYTIC METHODS

We start by reviewing the different analytic methods we consider—our goal is not to provide a comprehensive description of each method, but to provide an overview and highlight the relationships between the different methods.

A. Dynamics and linear theory

By far the most popular approach to an analytic description of large-scale structure is to approximate the matter distribution as an irrotational fluid, characterized by a density contrast $\delta(x) = \rho(x)/\bar{\rho} - 1$ and a peculiar velocity divergence $\theta(x) = \nabla \cdot v(x)$. The fluid equations, in Fourier space, are then (see Appendix A for a detailed derivation)

$$\frac{\partial \delta(k)}{\partial \tau} + \theta(k) = -\int \frac{d^3q}{(2\pi)^3} \frac{k \cdot q}{q^2} \theta(q)\delta(k - q), \tag{1a}$$

$$\frac{\partial \theta(k)}{\partial \tau} + \mathcal{H}\theta(k) + \frac{3}{2}\Omega_m \mathcal{H}^2\delta(k) = -\int \frac{d^3q}{(2\pi)^3} \frac{k^2 q \cdot (k - q)}{2q^2|k - q|^2} \theta(q)\theta(k - q). \tag{1b}$$

Here $d\tau = dt/a(t)$ is conformal time, $\Omega_m(\tau) = \bar{\rho}(\tau)/\rho_{\rm crit}(\tau)$, and $\mathcal{H} = aH$ is the conformal Hubble parameter. [Note that we adopt the Fourier transform convention that puts the $(2\pi)^3$ in the wave vector integral. We also omit the tilde that is usually used to decorate Fourier space quantities.] The nonlinear nature of these equations is manifest in the mode-coupling integrals.

Working to linear order in δ and θ, we obtain

$$\delta_L(k; z) = \frac{D(z)}{D(z_i)}\delta_i(k) \tag{2}$$

and

$$\theta_L(k; z) = -\mathcal{H}(z)f(z)\frac{D(z)}{D(z_i)}\delta_i(k), \tag{3}$$

where δ_i is the density contrast at some early time z_i when linear theory is certainly valid, D is the linear growth function (normalized to 1 at $z = 0$), and $f \equiv d\ln D/d\ln a$. At early times $\Omega_m \approx 1$ and $D \propto a$. For convenience we define δ_0 to be the linear density contrast today, i.e. $\delta_0(k) = \delta_L(k; z = 0)$. When convenient we also follow common practice and use $\eta = \ln D$ as a time variable; for brevity we often suppress the time dependence of quantities altogether. It is further convenient to group δ and θ into a two-component vector, $\Phi_a(k) = (\delta(k), -\theta(k)/\mathcal{H}f)$ which is proportional to $(1, 1)$ in linear theory.

B. Statistical observables

Inflation predicts, and observations have confirmed, that the initial fluctuations are predominantly adiabatic [10], almost scale invariant [10], and very close to Gaussian [11]. Under the assumption that the initial field is Gaussian all expectation values of moments of the evolved density and velocity fields can be expressed as integrals over the linear theory power spectrum. For example, the evolved two-point function

$$(2\pi)^3\delta_D(k + k')P_{ab}(k) = \langle \Phi_a(k)\Phi_b(k') \rangle, \tag{4}$$

whose components are all equal to $P_L(k)$ in linear theory, can be expressed as integrals over n powers of P_L in nth order perturbation theory [e.g. Eq. (A20)].

In general, to give a complete statistical description of the matter distribution at a given time, one would need to specify the entire hierarchy of connected n-point correlators. For initially Gaussian fields which are close to linear, the higher-order connection functions are small and have been compared to simulations in [12]. We shall confine our attention to the two-point function in this paper.

The nonlinear propagator [13,14] (also known as the response function [5]) measures the correlation between the evolved field $\Phi_a(k; \eta)$ and the initial conditions $\Phi_a(k; \eta_i)$. It is formally defined as a functional derivative,

$$\delta_D(\boldsymbol{k} - \boldsymbol{k}')G_{ab}(k; \eta, \eta_i) = \left\langle \frac{\delta\Phi_a(\boldsymbol{k}; \eta)}{\delta\Phi_b(\boldsymbol{k}'; \eta_i)} \right\rangle, \quad (5)$$

though its significance is easier to understand from the relation

$$\langle\Phi_a(\boldsymbol{k}; \eta)\Phi_b(\boldsymbol{k}'; \eta_i)\rangle = G_{ac}(k; \eta, \eta_i)$$
$$\times \langle\Phi_c(\boldsymbol{k}; \eta_i)\Phi_b(\boldsymbol{k}'; \eta_i)\rangle, \quad (6)$$

which we shall take as a definition henceforth. At early times or at large scales, there is near-perfect correlation ($G_{ab} \approx 1$), but $G_{ab} \rightarrow 0$ on small scales as nonlinear evolution washes out the initial conditions [15,16].

Because we will make reference to it later, we also introduce here the quantity

$$\Sigma^2 \equiv \frac{1}{3\pi^2} \int_0^\infty dq P_L(q), \quad (7)$$

which characterizes the scale at which nonlinearities become important. In the Lagrangian formalism (see below) Σ^2 gives the variance of each component of the linear (or Zel'dovich) displacement.

C. Beyond linear theory

The program is now to compute the statistics of the evolved density field in terms of the initial density field. This is simple in principle but difficult in practice, because the equations of motion are both nonlinear and nonlocal (in both configuration space and Fourier space). Nonlinearity forces one to seek a perturbative solution, since exact solutions to Eqs. (1) (even if they could be found) could not be combined to construct a realistic solution. A straightforward perturbative approach is hampered by computational costs, as nonlocality implies that higher-order terms involve mode-coupling integrals of ever higher dimension.

This situation has prompted a study of higher-order methods for statistical observables like the power spectrum. Many of these methods were borrowed from other areas of physics (notably particle physics and fluid mechanics [17]) where they achieved mixed success. We review these below, highlighting the relationships between the different methods; the methods we consider are summarized in Table II.

The most straightforward approach is to define a series solution to the fluid equations in powers of the initial density field δ_i (or equivalently, the linearly evolved density field, δ_0). This is the basis behind *standard perturbation theory* (hereafter SPT [18–23]); a detailed description (including explicit expressions for P_{ab} to third order in P_L) is presented in AppendixA.

Comparisons with simulations (including those presented below) have shown that the domain of applicability of second order (in P_L) perturbation theory is rather small at $z \approx 0$. Furthermore, as we show below, going to third

order is not guaranteed to improve agreement, leading one to question the convergence properties of such a series expansion. If one could carry out any expansion to infinite order it would (trivially) give the correct answer. This however is usually not possible. This has led various authors to investigate ways of summing subsets of the terms to arbitrary order in some expansion coefficient.

Renormalized perturbation theory (hereafter RPT, see [13,14,25]) is a variant of Dyson-Wyld resummation (see [17] for a discussion in the context of hydrodynamics) and attempts to reorganize the perturbation expansion in terms of the nonlinear propagator and nonlinear vertex to improve convergence. In particular, if the vertex is approximated by its tree-level form then the power spectrum can be written as an expansion in the nonlinear propagator. The resulting series is therefore no longer an expansion in powers of the initial density contrast, but rather "an expansion in orders of the complexity of the interaction" [29].

In [14] the dominant contributions to the nonlinear propagator are identified and summed explicitly in the high-k limit, giving $G_{ab} \sim e^{-\Sigma^2 k^2/4}$ for large k (see also [15,16]). Matching this behavior with the one-loop propagator (valid at low k) gives a nonperturbative prediction for G_{ab}. Substituting this propagator in the first few diagrams of the reorganized expansion then gives a nonperturbative prediction for the power spectrum [25]. We implemented the one-loop and two-loop mode-coupling contributions as described in [25].

The above methods work at the level of the density and velocity fields; an alternative approach is to use the fluid equations to derive equations of motion for the power spectrum and higher-order correlators directly. Such an approach results in an infinite hierarchy of equations, which must be somehow truncated. The *closure theory* approach [3] does so by approximating the three-point correlator $\langle\Phi_a\Phi_b\Phi_c\rangle$ by its leading order expression in SPT. As in [14], G_{ab} can be computed explicitly in the low-k and high-k limits, and matched naturally in intermediate regimes. The power spectrum is then obtained order by order via a Born-like series expansion.

A variant of this approach (hereafter time-RG theory [26]) assumes a vanishing trispectrum to truncate the hierarchy. The resulting equations of motion for the power spectrum P_{ab} and bispectrum B_{abc} can then be numerically integrated forward in time, starting at some sufficiently early redshift z_i (where $P = P_L$ and $B = 0$). Since the time evolution is performed numerically, the method also allows the proper treatment of models where the linear growth factor is scale dependent (e.g. models with quintessence or massive neutrinos [30]). This approach may be seen as a generalization of the *renormalization group perturbation theory* (hereafter RGPT) of [31], which is an attempt to regulate the relative divergence of one-loop SPT using renormalization group methods.

In [32–34] a path-integral formulation of the Vlasov equation is developed in terms of the distribution function $f(\mathbf{x}, \mathbf{p}, t)$. In [27] a similar technique is applied to the fluid equations [Eq. (A10)]. The key insight here is that statistical observables like the power spectrum may be obtained by taking functional derivatives of an appropriately constructed path integral (the generating functional). Straightforward perturbative evaluation of the generating functional reproduces the results of SPT, whereas applying large-N expansion techniques and truncating at fixed order in $1/N$ leads to approximations for the power spectrum and propagator. These approximate solutions agree with SPT up to a fixed order in P_0, but also include nonperturbative contributions corresponding to infinite partial resummations of the standard expansion. We focus attention on the steepest-descent method of [27] (hereafter large-N), as it is considerably easier to implement than the 2PI effective action method. (At one-loop order the 2PI method gives the same results as closure theory [35].)

Lagrangian resummation theory (hereafter LagR, [28,36]) is an extension of the well-developed Lagrangian perturbation theory. Lagrangian perturbation theory (hereafter LPT; see [37–39]) has received less attention recently than its Eulerian counterpart as a method for investigating nonlinear structure growth, partly because the Lagrangian picture breaks down once shell crossing occurs. However, recent work [28] has demonstrated that Lagrangian perturbation theory not only reproduces the SPT power spectrum at the lowest nontrivial order, but with a slight modification also yields a nonperturbative prediction for the power spectrum that corresponds to resumming an infinite set of terms in the standard expansion. We review LPT and the cumulant expansion in Appendix B.

III. SIMULATIONS

In order to assess how well the perturbative expansions are doing, we need a reference for any given cosmology. We use a new set of large dynamic range N-body simulations well suited to this purpose. These computer programs simulate the same basic physical system (a collisionless matter "fluid" interacting only through gravity) that the perturbative methods attempt to describe; hence the results of the two methods, though arrived at very differently, are directly comparable.

We have elected to investigate several different cosmologies, in an attempt to better identify where and why various analytic techniques succeed and/or fail. For simplicity we consider only flat models in the cold dark matter (CDM) family. We will highlight two: the first in which a cosmological constant dominates the late-time evolution and which is close to the best-fit cosmology (ΛCDM: $\Omega_M = 0.25$, $\Omega_b h^2 = 0.0224$, $h = 0.72$, $n = 0.97$, and $\sigma_8 = 0.8$) and an extreme model (cCDM: $\Omega_M = 1$, $\Omega_b h^2 = 0.1$, $h = 0.5$, $n = 1$, and $\sigma_8 = 1$) with a critical

TABLE I. The value of the dimensionless, linear power spectrum at $z = 1$ and $z = 0$ at several fiducial wave numbers for our two example cosmologies. k is given in h Mpc^{-1}.

k	$\Delta_L^2(z = 1)$		$\Delta_L^2(z = 0)$	
	ΛCDM	cCDM	ΛCDM	cCDM
0.05	0.03	0.03	0.09	0.14
0.10	0.11	0.09	0.27	0.36
0.15	0.19	0.22	0.49	0.90
0.20	0.29	0.27	0.72	1.07
0.25	0.37	0.38	0.94	1.51

density in matter and a larger present-day normalization which emphasizes the effects of nonlinearity and the erasure of baryon acoustic oscillations through mode coupling.

For each cosmology the transfer function, $T(k)$, was computed by evolving the coupled Boltzmann, fluid, and Einstein equations using the publicly available package CAMB [40]. The resulting power spectra were then used both as input to the perturbative methods and to generate initial conditions for the N-body simulations (Table I gives the amplitude of the dimensionless power at some fiducial wave numbers).

A number of numerical issues need to be addressed in order to ensure that our simulations provide an adequate reference. Our workhorse simulations each employ 1024^3 equal mass dark matter particles in a periodic, cubical box of side length $2h^{-1}$ Gpc. By employing such large volumes we are highly insensitive to the periodicity of the box, which represents a fair sample of the Universe [9]. There is very little power at the fundamental mode, even at $z = 0$: $\Delta^2(k_f, z = 0) < 10^{-4}$. The lowest few modes obey linear growth to sub-percent accuracy and we run enough different realizations to ensure that the spectrum at the scales of interest is well determined. The large number of particles ensures that the spectrum is well converged for the k modes of interest, which we checked explicitly by comparing simulations of different box sizes. The simulations are evolved from $z_i = 100$, with the particles perturbed from an initially uniform grid using the Zel'dovich approximation. The rms particle move was about 5% of the mean interparticle spacing. Comparison with second order Lagrangian perturbation theory initial conditions showed that this starting redshift is sufficiently high that transients from the Zel'dovich start are irrelevant for the scales and redshifts of interest.

Most of the evolutions were performed with a parallel particle-mesh code. To cross-check our results we used two high force resolution N-body codes: the TreePM code [41] and GADGET-II [42]. These have each been tested against a suite of other codes [7–9], with very good agreement. We ran a subset of our simulations using all three codes to quantify the level of precision for the box size and particle loading of relevance here. With its default time stepping,

the TreePM code produces dark matter power spectra in agreement with those from GADGET-II to better than 0.2% out to $k \simeq 1h$ Mpc^{-1} and to $\mathcal{O}(10^{-4})$ for $k < 0.1h$ Mpc^{-1}. However, these runs prove to be quite time consuming. If we set the time step in the TreePM code to

$$(\delta \ln a)^{-2} = \left[\frac{1}{0.05}\right]^2 + \left[\frac{a}{0.01}\right]^2, \qquad (8)$$

which evolves from 5% steps at early times to 1% steps as $a \rightarrow 1$, we find a shortfall of power of approximately 1% at $k \simeq 1h$ Mpc^{-1} but very little difference for $k < 0.1h$ Mpc^{-1}. We choose the same time stepping for the particle-mesh code, which results in very short run times allowing an ensemble of simulations to be performed. With this step the particle-mesh power spectra show a significant deficit of power (compared to TreePM or GADGET-II) be-

yond $k \approx 0.7h$ Mpc^{-1} but for $k < 0.2h$ Mpc^{-1}, the region of interest here, the agreement is better than 1%.

To compute the power spectrum at different output times, the particles were binned onto a regular, Cartesian grid using charge-in-cell assignment [43] and the resulting density field was Fourier transformed. The Fourier modes were squared, corrected for the gridding by dividing by the Fourier transform of the charge assignment scheme, and binned into bins equally spaced in $\log k$. The average of $\Delta^2(k)$ was assigned to the average k in the bin and shot noise was subtracted assuming it was Poisson. The binning introduces artifacts at low k, where the sampling on the grid is sparse and the dimensionless power spectrum is steep, but these are small for the scales of most relevance to us. Similarly there is some evidence that the shot noise in simulations is not scale invariant (Poisson), but the correction is negligibly small on the scales of interest here.
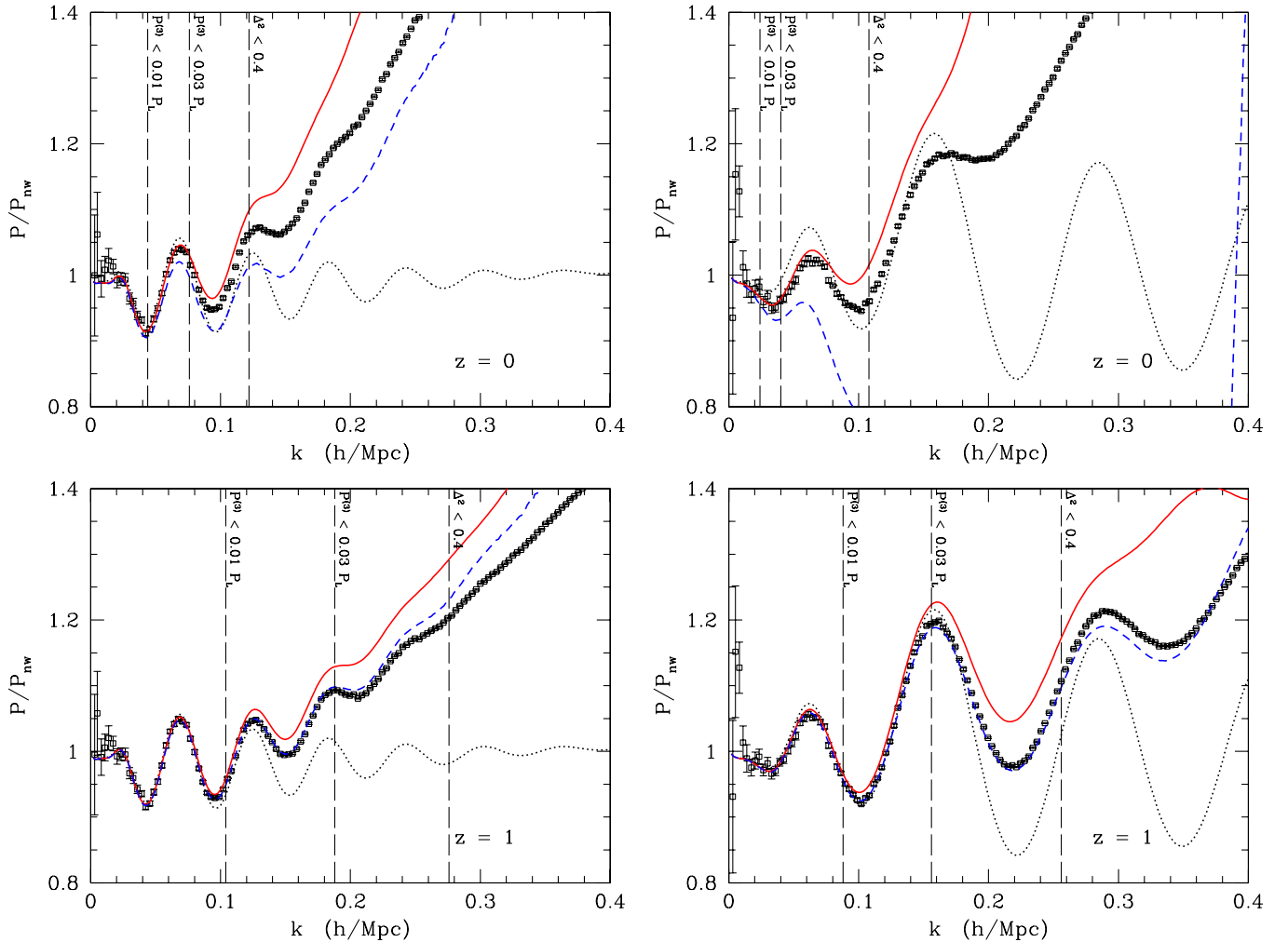

FIG. 1 (color online).   SPT power spectrum at linear (black; dotted), one-loop (red; solid), and two-loop (blue; dashed) order. The squares with error bars show the mean and error from our N-body simulations. The four panels show ΛCDM (left) and cCDM (right) at redshifts 0 (top) and 1 (bottom). Each curve has been divided by the no-wiggle power spectrum of [60] to reduce the dynamic range. We also indicate the domain of validity of one-loop SPT according to the heuristic prescription of [45] ($\Delta^2 < 0.4$), and according to the criterion $P^{(3)} < \alpha P_L$ for $\alpha = 0.01, 0.03$.

The nonlinear propagator was computed by cross correlating the initial density field with the final one [14]. Similar to the power spectrum, this quantity is obtained by Fourier transforming both fields, multiplying their Fourier coefficients, correcting for gridding, and then binning the results.

The velocity statistics are more problematic, because while the density and momentum fields must vanish where there are no tracer particles, the same is not true of the velocities. Thus estimates of the velocity field must employ a smoothing technique. Similarly, the velocity field is more sensitive to finite force resolution. On the other hand, comparison of the velocity fields with the density fields is less sensitive to finite volume scatter. For this reason we use a different set of simulations, with more particles (up to three billion) in smaller boxes ($1.25h^{-1}$ Gpc down to $720h^{-1}$ Mpc) evolved with the TreePM code, for the velocity statistics. Comparison with different smoothing

schemes, box sizes, and particle loadings show that with these choices our results are well converged on the scales of interest [44].

IV. COMPARISON

A. The power spectrum

We begin our analysis by comparing the predictions of SPT against our simulation results. Figure 1 shows the linear theory, one-loop SPT, and two-loop SPT power spectrum for ΛCDM and cCDM. While two-loop SPT is a marked improvement over one-loop SPT at $z = 1$, it is actually worse than one-loop at $z = 0$. The effect is most apparent in cCDM, which has larger σ_8 and Ω_b. This breakdown in standard perturbation theory is not entirely surprising: since the nth order term in SPT goes like $D^{2n}(z)$, at any given scale one expects higher-order terms to become comparable in magnitude to lower order terms
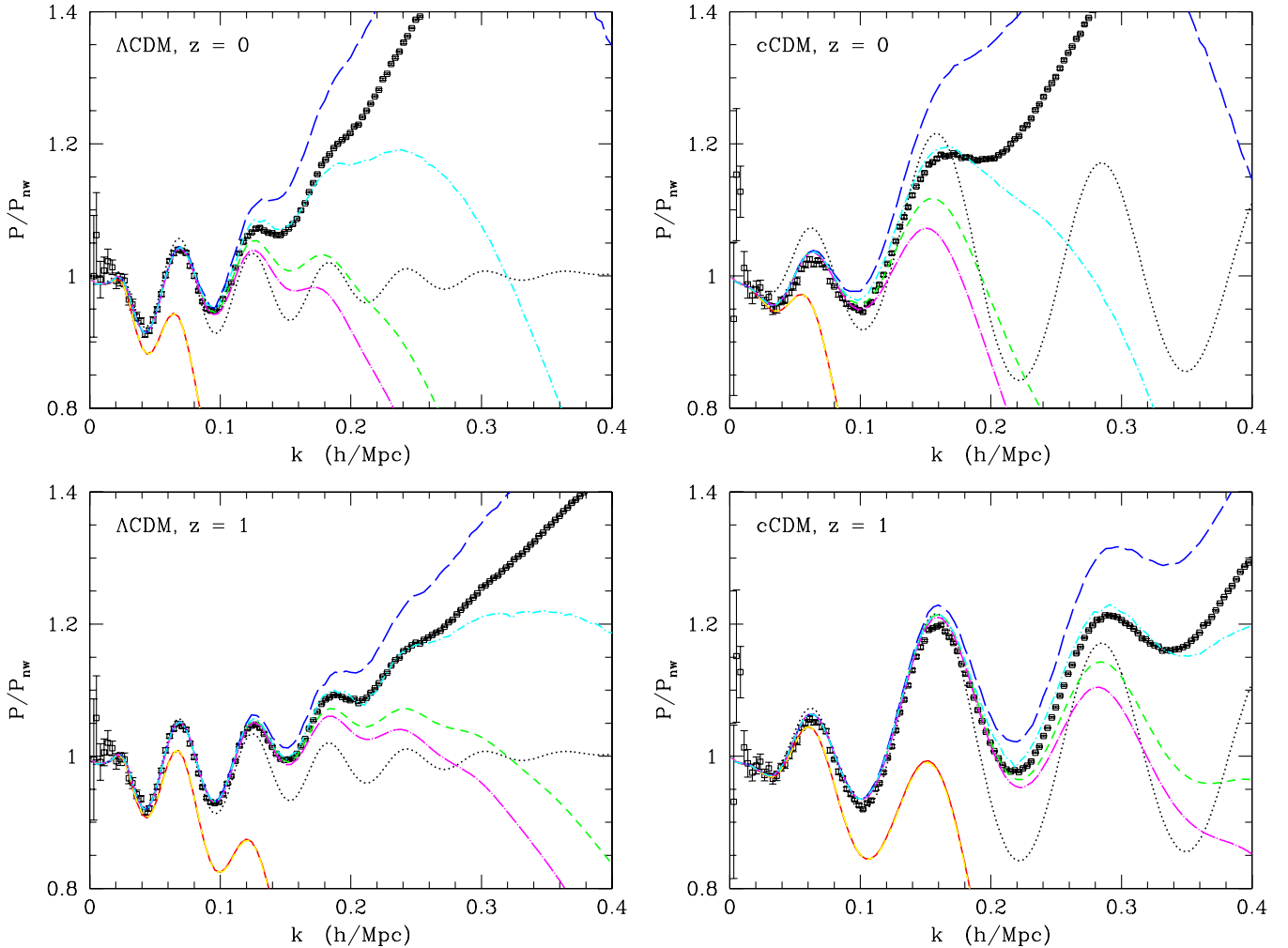

FIG. 2 (color online). Comparison of the tree-level, one-loop and two-loop power spectrum from RPT and closure theory, for ΛCDM (left) and cCDM (right). Each curve has been divided by the no-wiggle power spectrum of [60] to reduce the dynamic range. The (black) dotted line is linear theory, the (red) solid line is tree-level RPT, the (green) dashed line is one-loop RPT, the (blue) long-dashed line is two-loop RPT, the thick (yellow) short-long-dashed line is tree-level closure, the (magenta) dot-long-dashed line is one-loop closure, and the (cyan) dot-dashed line is two-loop closure.

at sufficiently late times. Our results suggest that at BAO scales (roughly $k = 0.05$–$0.25h$ Mpc^{-1}) the breakdown occurs between $z = 1$ and $z = 0$.

A common heuristic prescription dictates that one-loop SPT can be trusted to 1% for wave numbers satisfying $\Delta_L^2(k) \lesssim 0.4$ [45]. On the other hand, a strict application of perturbation theory implies that one-loop SPT can be trusted to 1% for wave numbers where the two-loop contribution is 1% of linear theory. In Fig. 1 we indicate the predicted domain of validity of one-loop SPT according to these two criteria. For comparison, we also indicate where the two-loop contribution is within 3% of linear theory. One sees that the agreement with simulations is slightly better than what our more rigorous criterion suggests. For instance, for ΛCDM at $z = 0$, $\Delta_L^2 = 0.4$ at $k_* \approx 0.12h$ Mpc^{-1}. At this wave number one-loop SPT overshoots the reference spectrum by about 3%, whereas two-loop SPT undershoots the reference spectrum by 5%. For

cCDM at $z = 0$ the situation is much worse, with one-loop SPT overshooting by only 6% at $k_* \approx 0.11h$ Mpc^{-1}, but two-loop SPT undershooting by almost 20%.

RPT and closure theory have also been developed to two loops. Given the above conclusions about SPT, it is natural to make the same comparison between the one-loop and two-loop predictions from RPT and closure theory. In Fig. 2 we show the matter power spectrum for these theories at tree, one-loop, and two-loop order for both ΛCDM and cCDM. For closure theory it appears that going to two-loop order extends the range of agreement with simulations, although the wiggles of the power spectrum are not matched in detail. For RPT, as with SPT, the two-loop result is systematically high, whereas the one-loop result performs fairly well below $k \approx 0.15h$ Mpc^{-1}. Agreement with simulations can be improved by changing the damping scale in the propagator. In [25] the damping scale was modified by calculating Σ with the linear theory
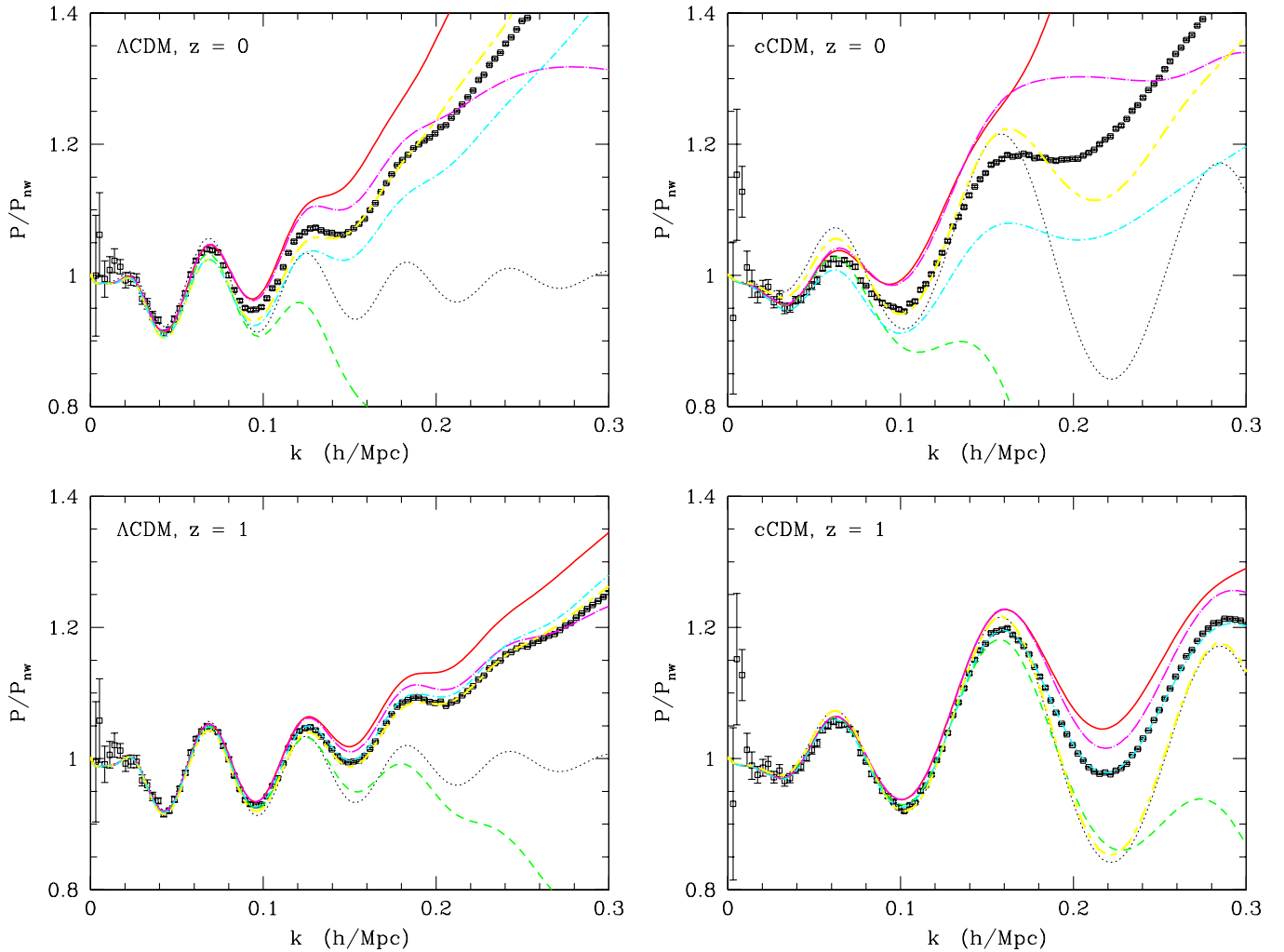

FIG. 3 (color online).   Comparison of the power spectrum for the remaining theories. Each curve has been divided by the no-wiggle power spectrum of [60] to reduce the dynamic range. The (red) solid line is one-loop SPT, the (magenta) dot-long-dashed line is large-N theory, the (green) dashed line is Lagrangian resummation, the thick (yellow) short-long-dashed line is time-RG theory, and the (cyan) dot-dashed line is RGPT.

expression [Eq. (7)], but using the nonlinear power spectrum and integrating only up to $k = 4k_{nl}$. This leads to a $\sim 10\%$ additional suppression of $G(k)$ and hence $P(k)$ on the relevant scales, bringing the theory into better agreement with simulations [25]. At present this correction has not been derived from first principles and we have not included it, but it appears that improvements in this direction could be important.

Figure 3 shows the predicted power spectrum for the remainder of the theories that we consider in this work. With Figs. 1 and 2, these figures give an overview of the agreement between our N-body simulations and the perturbation theories for ΛCDM and cCDM. Some of the trends can be seen easily in these figures, and are generic across cosmologies and redshifts. For instance, one-loop SPT, which is the same as one-loop LPT, always overpredicts $P(k)$ at high k. Lagrangian resummation theory on the other hand is much too strongly damped beyond the first wiggle. Large-N theory more or less traces one-loop SPT before turning over, while time-RG theory and RGPT follow the general trends of the N-body data without fitting any particular feature precisely. (Note that the nearly perfect agreement between RGPT and simulations for cCDM at $z = 1$ is likely spurious, as this level of agreement is not seen for other cosmologies or at other redshifts.) RPT and closure give nearly identical tree-level predictions, and very similar one-loop predictions for $P(k)$. Closure theory appears to benefit greatly from going to two-loop order, whereas for RPT even at $z = 1$ it appears that two-loop does worse than one-loop.

While we have run many realizations of each cosmology to reduce run-to-run variance, one sees in Figs. 1–3 that the N-body data are still noisy at low k, which makes it difficult to make quantitative statements about the performance of the perturbation theories. To overcome this we define a "reference spectrum" which interpolates the N-body results at high and intermediate k with the one-loop SPT calculation at low k. This eliminates the large scatter from the finite number of modes in the simulations and any biases from the finite bin sizes at low k, while still retaining the information from the simulations at larger k. This gives a smooth function, defined for all k, which can be used as a reference to make a quantitative comparison. Given the large number of simulations we have run, the uncertainty in the N-body results is small before perturbation theory becomes invalid and we can see a significant range of k for which theory and simulation agree well. This makes our final results insensitive to how the matching is done. Our recipe for producing a reference spectrum is to treat both the N-body results and one-loop SPT as independent measurements of the true power spectrum, with errors given by the run-to-run variance within a wave number bin [46] in the former case, and by the two-loop SPT term in the latter case. Then the reference spectrum at any given k is defined by fitting a polynomial to all avail-
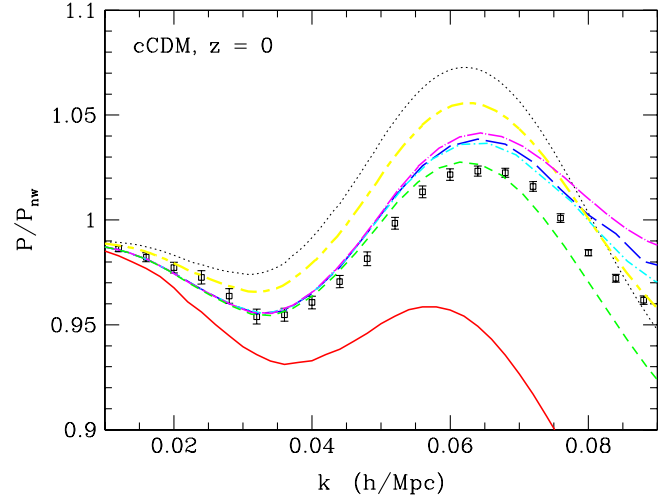

FIG. 4 (color online). Comparison between analytic models for $P(k; z = 0)$ and the reference spectrum (Sec. IV) for model cCDM, focusing on large scales. Each curve has been divided by the no-wiggle power spectrum of [60] to reduce the dynamic range. The points with error bars are the "reference spectrum" defined in the text. The (black) dotted line is linear theory, the (red) solid line is two-loop SPT, the (blue) long-dashed line is two-loop RPT, the (green) short-dashed line is Lagrangian resummation, the (cyan) dot-dashed line is two-loop closure theory, the thick (magenta) dot-long-dashed line is the large-N expansion, and the thick (yellow) short-long-dashed line is time-RG theory.

able measurements within a small wave number range [$k - \Delta k$, $k + \Delta k$] and evaluating that polynomial at k. For simplicity we chose to fit to a cubic with $\Delta k = 0.01h$ Mpc^{-1}, though the resulting reference spectrum is rather insensitive to these choices.

All of the theories beyond linear correctly predict the "dip" below linear theory which can be most clearly seen in Fig. 4 around $k \simeq 0.04h$ Mpc^{-1}. This is sometimes

TABLE II. The methods we consider in this work and the lowest k (in h Mpc^{-1}) at which each method departs from our reference spectrum by 1%, as a function of redshift for our chosen ΛCDM cosmology.

		$k_{max}(z)$				
		$z = 0$	0.3	0.7	1	1.5
Methods		$D = 1$	0.87	0.72	0.63	0.52
Linear		0.03	0.08	0.09	0.09	0.09
One-loop SPT	[18–23]	0.08	0.10	0.11	0.13	0.14
Two-loop SPT	[24]	0.04	0.06	0.09	0.23	0.20
One-loop RPT	[13,14,25]	0.10	0.13	0.15	0.16	0.20
Two-loop RPT		0.08	0.08	0.11	0.11	0.13
One-loop closure	[3]	0.09	0.10	0.14	0.15	0.18
Two-loop closure		0.08	0.13	0.17	0.27	0.21
Time-RG	[26]	0.04	0.05	0.06	0.09	0.10
Large-N	[27]	0.08	0.11	0.12	0.14	0.17
LagR	[28]	0.07	0.08	0.09	0.10	0.13

TABLE III. The value of k, in $h\,\mathrm{Mpc}^{-1}$, to which various flavors of perturbation theory can be trusted according to various published criteria. See [2] for discussion.

Reference	Method	ΛCDM		cCDM	
		$z = 0$	$z = 1$	$z = 0$	$z = 1$
[45]	SPT	0.12	0.28	0.07	0.25
[47]	SPT	0.10	0.19	0.08	0.19
[2]	SPT	0.08	0.09	0.08	0.09
[28]	LagR	0.08	0.13	0.07	0.15
[2]	RPT	0.09	0.09	0.09	0.10
[2]	Closure	0.09	0.09	0.09	0.10

referred to as previrialization, and arises because the nonlinear growth of the density and velocity fields is slower than linear on scales where the effective spectral index is more positive than (about) -1.5 (see [12] for further discussion). In this region use of any of the methods provide significant improvements over linear theory.

To gain an overview of the range of validity of the various methods, we list in Table II the smallest value of k at which each method departs from our reference spectrum by 1% for ΛCDM (a comparison with other schemes defined in the literature is presented in Table III). As expected, the methods perform better at smaller scales the higher the redshift. All of the methods outperform linear theory, owing to the marked effects of previrialization, however none of the methods appear to be accurate beyond $k \simeq 0.1h\,\mathrm{Mpc}^{-1}$ at $z = 0$.

In Fig. 5 we show the fractional residuals of each theory compared to our reference spectrum for the ΛCDM cosmology at $z = 0$ and $z = 1$. The effects of previrialization

are clearly visible between $k = 0.02h\,\mathrm{Mpc}^{-1}$ and $k = 0.07h\,\mathrm{Mpc}^{-1}$.

B. Testing the dynamics

While comparison of the power spectrum is the most common test for perturbation theory, it is also useful to test if perturbation theory is correctly describing the underlying dynamics. To do so, we examine some of the constituent pieces from the simulations, and compare to the perturbation theory predictions.

Figure 6 compares the nonlinear propagator

$$\tilde{G}_1(k) = G_{11}(k) + G_{12}(k) \sim \frac{\langle \delta_{\mathrm{NL}} \delta_L^* \rangle}{\langle \delta_L \delta_L^* \rangle} \qquad (9)$$

from the simulations with the predictions of analytic models. Only RPT and Lagrangian resummation give the expected behavior, $\tilde{G}_1 \to 0$, for large k.

Comparisons of perturbation theory with simulations typically focus on the density autocorrelation function or power spectrum. However, perturbation theory also makes predictions for the (irrotational) velocity field which can be checked against simulations. In Fig. 7 we show the cross-correlation coefficient

$$r(k) \equiv P_{\delta\theta}(k)/\sqrt{P_{\delta\delta}(k)P_{\theta\theta}(k)} \qquad (10)$$

for several theories, compared with the same quantity measured from simulations. In linear theory $r(k) = 1$ identically. On physical grounds, one expects to see a decoherence of density and velocity fields on small scales, and indeed the simulations show $r(k) \to 0$ for large k. None of the analytic theories correctly reproduce this behavior. SPT
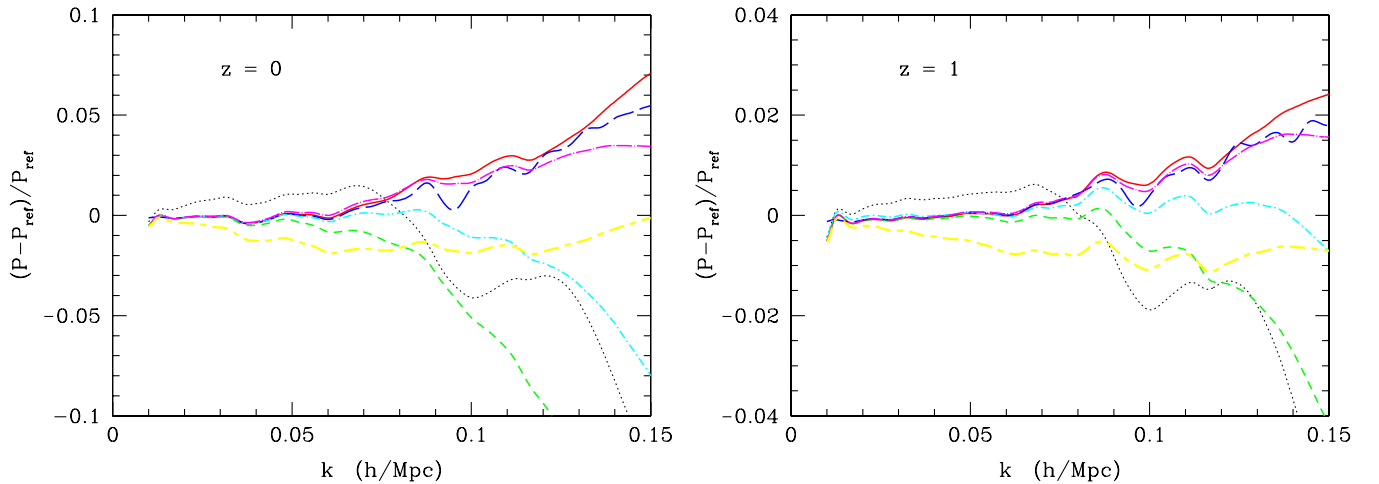

FIG. 5 (color online). The fractional deviation of each method from the reference spectrum, for ΛCDM at $z = 0$ (left) and $z = 1$ (right). This figure focuses on the region $k < 0.15h\,\mathrm{Mpc}^{-1}$ where linear theory is inadequate but higher-order methods are still viable. As in Fig. 4 the (black) dotted line is linear theory, the (red) solid line is two-loop SPT, the (blue) long-dashed line is two-loop RPT, the (green) short-dashed line is Lagrangian resummation, the thick (cyan) dot-short-dashed line is two-loop closure theory the thick (magenta) dot-long-dashed line is the large-N expansion, and the thick (yellow) short-long-dashed line is time-RG theory.
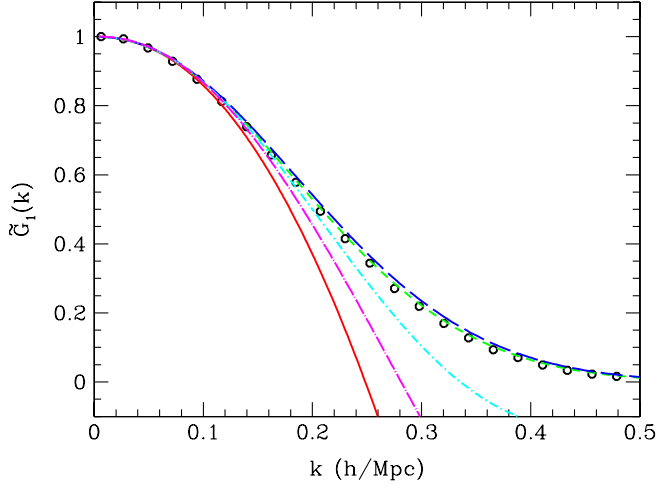
FIG. 6 (color online). The nonlinear propagator (normalized to 1 at $k = 0$) for ΛCDM at $z = 0$. The (red) solid line is SPT, the (green) short-dashed line is Lagrangian resummation, the (blue) long-dashed line is RPT, the thick (cyan) dot-short-dashed line is closure theory and the thick (magenta) dot-long-dashed line is the large-N expansion.

and time-RG theory follow the downward turn of the simulation data initially, but then predict an unphysical $r(k) > 1$ very soon after nonlinear corrections become important. RPT and closure theory perform somewhat
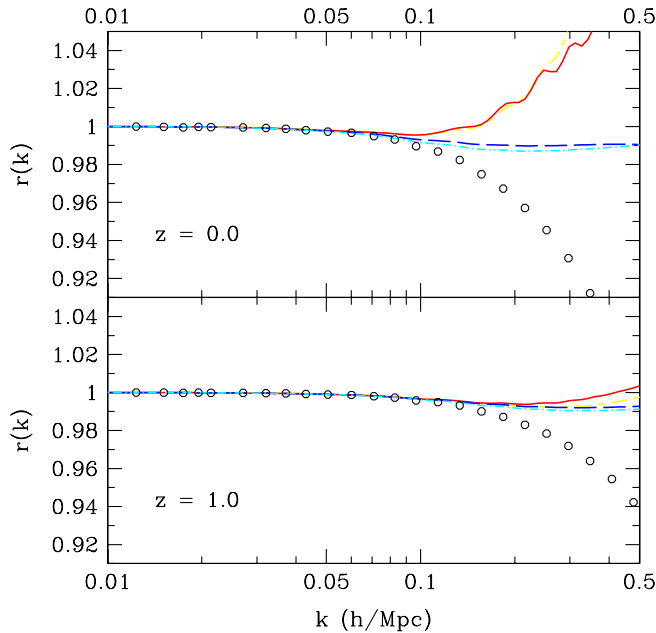

FIG. 7 (color online). A comparison of the density-velocity cross correlation predicted analytically with that measured in simulations, for ΛCDM at redshift $z = 0$ (top) and $z \approx 1$ (bottom). As in Fig. 4, the solid (red) line is SPT, the dashed (blue) line is RPT, the dot-dashed (cyan) line is closure theory, and the short-long-dashed (yellow) line is time-RG theory. For simplicity we show only the one-loop predictions for SPT, RPT, and closure theory.

better, in that $r(k)$ never exceeds unity, but the level of agreement with simulations is still not good above $k \simeq 0.1h$ Mpc^{-1}. (Note that we have displayed here only the one-loop predictions from these theories.) The deviation in $r(k)$ seems to be driven mostly by the densities, with perturbation theory performing better at the same scale for the velocities than the densities (see Fig. 8).

V. DISCUSSION

Standard perturbation theory has a simple and direct theoretical motivation, and results in explicit integral expressions at any order. If taken to infinite order, it provides an exact solution (though to an idealized problem). While standard perturbation theory works well at high redshift and large scales, our results indicate that the standard expansion is badly behaved at the redshifts and scales most accessible to observation, in that higher-order terms are comparable in magnitude to lower order terms. Although one expects the expansion to converge if taken to sufficiently high order, this comes at a great computational cost. With advances in raw computing power it may one day become possible to perform the calculation to the requisite order, but in the near future this approach seems impracticable.

On the other hand, it should be emphasized that SPT performs rather well at high redshifts, $z \gtrsim 1$. Figure 1 shows that two-loop SPT at $z = 1$ agrees with simulations to 1% out to $k = 0.2h$ Mpc^{-1} or beyond (where the simulations themselves become unreliable). At these redshifts SPT not only provides a reasonable theoretical prediction for the matter power spectrum on observationally relevant scales, but also an estimate of the theoretical uncertainty on this prediction.

RPT is essentially a rearrangement of the standard expansion, so like SPT it is an exact solution if carried out to all orders. While this rearrangement appears to improve the convergence properties of the perturbation series, it makes it unclear what small quantity (if any) we are actually expanding in. Furthermore, RPT does not actually provide closed-form expressions for the power spectrum, but rather integral relations where P_{ab} is expressed in terms of mode-coupling integrals of itself. Thus in addition to truncating the loop expansion at finite order, a fully consistent implementation of RPT requires solving for P_{ab} according to an iterative scheme, of which the explicit expressions presented in [25] represent only the first step. The error associated with this approximation has (to our knowledge) yet to be quantified.

Closure theory derives from a very different perturbative scheme than RPT, yet the results obtained are superficially quite similar. There is no obvious way to provide error estimates on the results of closure theory, however, as the closure equations are obtained from heuristic approximations rather than a systematic expansion. Furthermore the propagator in closure theory shows unrealistic oscillations
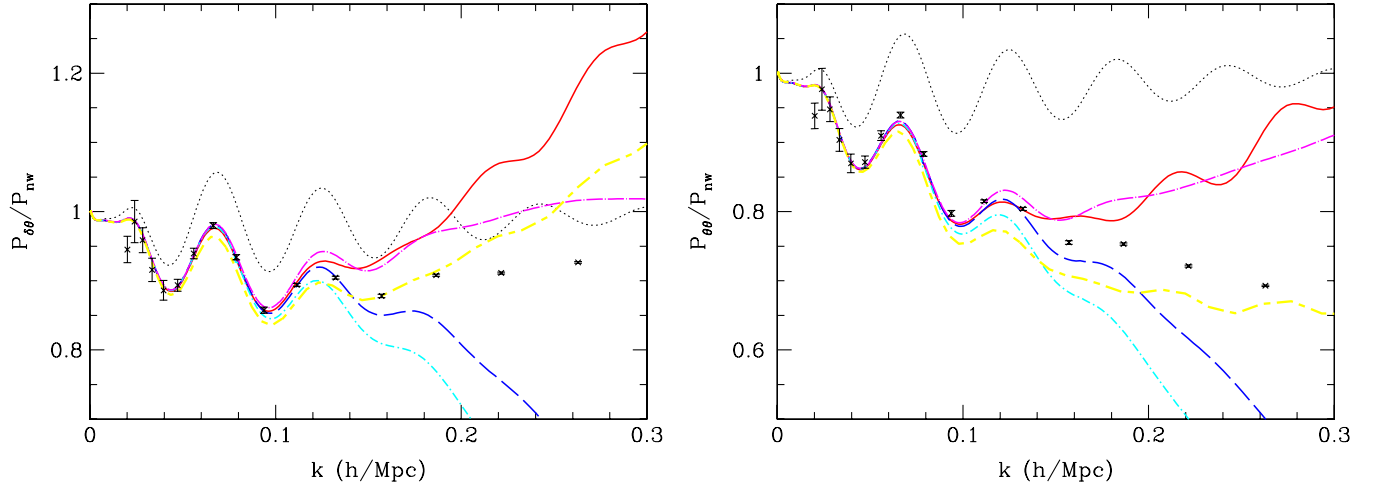
FIG. 8 (color online).   The density-velocity cross spectrum (left) and the velocity-velocity autospectrum (right) for the ΛCDM model at $z = 0$. As in Fig. 7 the (black) dotted line is linear theory, the (red) solid line is one-loop SPT, the (blue) long-dashed line is one-loop RPT, the (cyan) dot-short-dashed line is one-loop closure theory, the thick (magenta) dot-long-dashed line is large-N theory, and the thick (yellow) short-long-dashed line is time-RG theory.

for large k. As mentioned previously, the closure equations are solved approximately in [3] by means of a Born-like expansion. Recently [48] an attempt has been made to solve the closure equations numerically without resort to such a Born-like expansion. The resulting predictions for the power spectrum appear to agree better with simulations than the results presented here, although it is difficult to draw any firm conclusions from the information provided.

Time-RG theory is based on a single well-defined approximation: the vanishing of the trispectrum. The validity of this approximation can easily be checked in simulations, and in principle this could allow one to quantify the theoretical uncertainty in the method. As most easily seen in Fig. 5, although time-RG theory follows the general trends of our reference spectrum over a wider range than other methods, it comes up short by 1%–2% over the entire quasilinear regime. It also gives an unphysical prediction for the density-velocity cross correlation.

The large-N expansion utilizes more sophisticated theoretical machinery than other resummation techniques. While the path-integral formalism for computing clustering statistics is exact, the errors introduced by the large-N expansion are difficult to quantify, as "N" is a fictitious parameter. Although the large-N expansion corresponds to an infinite partial resummation of the standard perturbative expansion, from our results it seems that this resummation offers little improvement over one-loop SPT in the quasilinear regime. The grossly unphysical behavior of the propagator in this theory is likely responsible for this effect. As mentioned previously, we have focused attention on the steepest-descent method rather than the 2PI effective action method of [27]. The latter method produces a more reasonable propagator, and likely results in a better prediction for the power spectrum, although at an increased computational cost.

Like SPT, the Lagrangian resummation prescription of [28] also results in easy to compute, explicit integral expressions. These are well behaved at large k, allowing e.g. $\xi(r)$ to be computed, and there are natural extensions to redshift space and to halo bias [36]. For the real-space mass power spectrum considered here, it offers a marginal improvement over one-loop SPT for $k\Sigma < 1/2$, although the damping prefactor strongly overcompensates as one moves further into the quasilinear regime.

Our results have interesting implications for generating a suite of simulations aimed at constraining the matter power spectrum. If we can trust perturbative methods for $k\Sigma < x_c$, then we can focus the computational resources on higher k. Assuming Gaussian fluctuations, obtaining 1% accuracy in a bin $(k; \Delta k)$ requires 2×10^4 modes. There are $(kL_{\text{box}})^3(\Delta k/k)/(2\pi^2)$ modes from a periodic box of side length L_{box}, so our 1% constraint at $k\Sigma \simeq x_c$ translates into

$$L_{\text{box}} \simeq \frac{\Sigma}{x_c}\left(\frac{2\pi^2 N}{\Delta k/k}\right)^{1/3}$$
$$\approx 3 \text{ Gpc}\left(\frac{0.5}{x_c}\right)\left(\frac{\Sigma}{10 \text{ Mpc}}\right)\left(\frac{N}{2 \times 10^4}\right)^{1/3}\left(\frac{0.1}{\Delta k/k}\right)^{1/3} \tag{11}$$

or an equivalent volume of smaller simulations. This constraint is most difficult to meet at $z = 0$, since Σ is larger and the simulations must be evolved for longer. As an example with the default parameters listed above we would require 27 simulations, each $1h^{-1}$ Gpc on a side, to obtain percent level constraints on the power spectrum of ΛCDM in a 10% band near $k \simeq 0.1h$ Mpc^{-1} at $z = 0$ but at $z = 1$ we could trust perturbation theory at this scale and focus the simulations on $k \simeq 0.15h$ Mpc^{-1} where 3 times fewer simulations of the same size are needed.

TABLE IV.   Our input linear theory spectrum, at $z = 0$, for the ΛCDM model as a function of wave number (in h Mpc^{-1}) and the reference spectrum and propagator [$G(k)$] from our N-body simulations. Our convergence tests indicate the spectra should be accurate to $<1\%$ over the range of scales shown.

k	$\Delta_{\mathrm{lin}}^2(k)$	$\Delta_{\mathrm{ref}}^2(k)$	$G(k)$
0.02	0.012	0.012	0.996
0.04	0.053	0.053	0.980
0.06	0.130	0.129	0.950
0.08	0.210	0.210	0.914
0.10	0.274	0.285	0.859
0.12	0.398	0.410	0.804
0.14	0.466	0.507	0.737
0.16	0.533	0.617	0.664
0.18	0.662	0.764	0.592
0.20	0.720	0.894	0.518

VI. CONCLUSIONS

Perturbative methods have a long history in cosmology, and are widely used in many fields of physics. Many of the techniques reviewed herein were first developed in other fields and applied to other problems, with varying levels of success, before being pressed into service for modeling cosmological perturbations. In this paper we have studied a variety of these methods as applied to predicting the large-scale clustering of cold, collisionless matter in an expanding Universe. Our results indicate that the analytic theories correctly model the approach to nonlinearity and work well when the perturbations are small, but none of the available theories are up to the challenge of fully describing the behavior of matter on quasilinear scales at late times. We have emphasized the need to study a range of different cosmologies and to look at a variety of different statistical observables, as accidental agreement between theory and simulations is possible if one only considers the power spectrum. We have computed the two-loop contribution to SPT and found that the standard perturbative expansion is badly behaved at low redshifts, even on scales where one-loop SPT was previously believed to be valid. This provides further motivation for studying alternative analytic approaches based on nonperturbative methods, though at the same time it emphasizes the need for error control in analytic methods.

This work has made use of a large number of high dynamic range N-body simulations, against which we can compare the analytic models. We make these data public in Table IV to aid future work in the field. In addition, a flexible software package that implements the perturbation schemes described in this paper is available online [49].

ACKNOWLEDGMENTS

APPENDIX A: EULERIAN PERTURBATION THEORY

Here we briefly recap the derivation of the fluid equations in the Eulerian picture, and the assumptions that are made in perturbative treatments [18–23] (see [12] for a review). The matter content of the Universe is modeled as a large collection of identical particles of mass m, interacting only through mutual gravitational attraction. For low densities and subhorizon scales, such forces are adequately described by Newtonian gravity in a uniformly expanding background, with the Newtonian potential sourced by inhomogeneities in the density field. The distribution function for such a set of particles obeys the Vlasov equation. The N-body methods are essentially a Monte Carlo evolution of the Vlasov equation where the Monte Carlo tracer superparticles move along characteristics.

Analytically one typically invokes the *single-stream approximation*, which assumes that all particles at a given point x move together with the same velocity $v(x)$. This amounts to demanding that $f(x, p) \propto \delta_D[p - mav(x)]$, where f is the distribution function and δ_D is the Dirac delta function. This assumption is explicitly violated once shell crossing occurs in gravitational collapse (see [50] for a development of this idea), but is thought to be a reasonable approximation for small density contrasts. The velocity moments of the Vlasov equation then give the familiar fluid equations (e.g. [18])

$$\frac{\partial \delta}{\partial \tau} + \boldsymbol{\nabla} \cdot [(1 + \delta)\boldsymbol{v}] = 0, \tag{A1}$$

$$\frac{\partial \boldsymbol{v}}{\partial \tau} + \mathcal{H}\boldsymbol{v} + (\boldsymbol{v} \cdot \boldsymbol{\nabla})\boldsymbol{v} + \boldsymbol{\nabla}\Phi = 0, \tag{A2}$$

where $\mathcal{H} = d\ln a/d\tau = aH$ is the conformal Hubble parameter.

It is conventional to further assume that the vorticity $\boldsymbol{w} = \boldsymbol{\nabla} \times \boldsymbol{v}$ of the velocity field vanishes, i.e. that the fluid is *irrotational*. This assumption is motivated by noting that $\boldsymbol{w} \propto a^{-1}$ at linear order, and is well supported by simulations [51,52]. Under this approximation the velocity field is completely specified by its divergence $\theta = \boldsymbol{\nabla} \cdot \boldsymbol{v}$, and the fluid equations reduce to

$$\frac{\partial \delta}{\partial \tau} + \theta = -\boldsymbol{\nabla} \cdot (\delta \boldsymbol{v}), \tag{A3}$$

$$\frac{\partial \theta}{\partial \tau} + \mathcal{H}\theta + 4\pi G a^2 \bar{\rho}\delta = -\boldsymbol{\nabla} \cdot [(\boldsymbol{v} \cdot \boldsymbol{\nabla})\boldsymbol{v}]. \tag{A4}$$

In Fourier space $\boldsymbol{v}(\boldsymbol{k}) = -i\boldsymbol{k}\theta(\boldsymbol{k})/k^2$, giving

$$\frac{\partial \delta(\boldsymbol{k})}{\partial \tau} + \theta(\boldsymbol{k}) = -\int \frac{d^3 q_1 d^3 q_2}{(2\pi)^3} \delta_D(\boldsymbol{q}_1 + \boldsymbol{q}_2 - \boldsymbol{k})$$

$$\times \frac{\boldsymbol{k} \cdot \boldsymbol{q}_1}{q_1^2} \theta(\boldsymbol{q}_1)\delta(\boldsymbol{q}_2), \qquad (A5)$$

$$\frac{\partial \theta(\boldsymbol{k})}{\partial \tau} + \mathcal{H}\theta(\boldsymbol{k}) + \frac{3}{2}\Omega_m \mathcal{H}^2 \delta(\boldsymbol{k})$$

$$= -\int \frac{d^3 q_1 d^3 q_2}{(2\pi)^3} \delta_D(\boldsymbol{q}_1 + \boldsymbol{q}_2 - \boldsymbol{k})$$

$$\times \frac{k^2(\boldsymbol{q}_1 \cdot \boldsymbol{q}_2)}{2q_1^2 q_2^2} \theta(\boldsymbol{q}_1)\theta(\boldsymbol{q}_2). \qquad (A6)$$

As long as δ and θ are small, the right-hand sides of the fluid equations are small and can be dropped; this approximation defines linear theory. The solution to the resulting linearized fluid equations may be written as

$$\delta_L(\boldsymbol{k}; z) = \frac{D(z)}{D(z_i)}\delta_i(\boldsymbol{k}),$$

$$\qquad (A7)$$

$$\theta_L(\boldsymbol{k}; z) = -\mathcal{H}(z)f(z)\frac{D(z)}{D(z_i)}\delta_i(\boldsymbol{k}),$$

where δ_i is the density contrast at some early time z_i when linear theory is certainly valid, D is the linear growth function (normalized to 1 today), and $f \equiv d\ln D/d\ln a$. At early times $\Omega_m \approx 1$ and $D \propto a$. Note that a possible decaying mode contribution, proportional to $a^{-3/2}$ at early times, is forced to zero in linear theory by the condition that δ be well behaved as $a \to 0$. Note also that the mode-coupling integrals vanish for $\boldsymbol{k} = 0$, so linear theory is always valid in some neighborhood of $\boldsymbol{k} = 0$, even at late times. For convenience we define δ_0 to be the linear density contrast today, i.e. $\delta_0(\boldsymbol{k}) = \delta_L(\boldsymbol{k}; z = 0)$.

It often proves convenient to use $\eta = \ln D$ as a time variable, and to combine δ and θ into a two-component field

$$\Phi_a(\boldsymbol{k}) = \begin{pmatrix} \delta(\boldsymbol{k}) \\ -\theta(\boldsymbol{k})/\mathcal{H}f \end{pmatrix}. \qquad (A8)$$

If we introduce

$$\alpha(\boldsymbol{q}_1, \boldsymbol{q}_2) = \frac{\boldsymbol{k} \cdot \boldsymbol{q}_1}{q_1^2}, \qquad \beta(\boldsymbol{q}_1, \boldsymbol{q}_2) = \frac{k^2(\boldsymbol{q}_1 \cdot \boldsymbol{q}_2)}{2q_1^2 q_2^2}, \qquad (A9)$$

the fluid equations may be recast as

$$\left[\delta_{ab}\frac{\partial}{\partial \eta} + \Omega_{ab}\right]\Phi_b(\boldsymbol{k}; \eta)$$

$$= \int \frac{d^3 q}{(2\pi)^3}\gamma_{abc}(\boldsymbol{q}, \boldsymbol{k} - \boldsymbol{q})\Phi_b(\boldsymbol{q}; \eta)\Phi_c(\boldsymbol{k} - \boldsymbol{q}; \eta), \qquad (A10)$$

where

$$\Omega_{ab}(\eta) = \begin{pmatrix} 0 & -1 \\ -\frac{3\Omega_m}{2f^2} & \frac{3\Omega_m}{2f^2} - 1 \end{pmatrix} \qquad (A11)$$

and the vertex $\gamma_{abc}(\boldsymbol{q}_1, \boldsymbol{q}_2)$ only has nonzero entries $\gamma_{121}(\boldsymbol{q}_1, \boldsymbol{q}_2) = \gamma_{112}(\boldsymbol{q}_2, \boldsymbol{q}_1) = \alpha(\boldsymbol{q}_1, \boldsymbol{q}_2)/2$ and $\gamma_{222}(\boldsymbol{q}_1, \boldsymbol{q}_2) = \beta(\boldsymbol{q}_1, \boldsymbol{q}_2)$. The initial fields at time η_i are denoted

$$\phi_a(\boldsymbol{k}) \equiv \Phi_a(\boldsymbol{k}; \eta_i) = \delta_i(\boldsymbol{k})\begin{pmatrix} 1 \\ 1 \end{pmatrix}, \qquad (A12)$$

and the linear theory solution is simply $\Phi_a^{(L)}(\boldsymbol{k}; \eta) = e^{\eta - \eta_i}\phi_a(\boldsymbol{k})$.

1. Beyond linear order

Standard perturbation theory (hereafter SPT; [18–23]) defines a systematic series solution to the fluid equations (1) in powers of the initial density contrast δ_i (or equivalently in powers of the current linearly evolved density contrast δ_0). In an Einstein-de Sitter universe, where $\mathcal{H} \propto a^{-1/2}$ and $\Omega_m \mathcal{H}^2 \propto a^{-1}$, the expansion may be written as

$$\delta(\boldsymbol{k}; \tau) = \sum_{n=1}^{\infty} a^n(\tau)\delta_n(\boldsymbol{k}),$$

$$\qquad (A13)$$

$$\theta(\boldsymbol{k}; \tau) = -\mathcal{H}(\tau)\sum_{n=1}^{\infty} a^n(\tau)\theta_n(\boldsymbol{k}),$$

where $\delta_n(\boldsymbol{k})$ and $\theta_n(\boldsymbol{k})$ are time-independent mode-coupling integrals over n powers of the initial density field:

$$\begin{pmatrix} \delta_n(\boldsymbol{k}) \\ \theta_n(\boldsymbol{k}) \end{pmatrix} = \int \frac{d^3 q_1 \ldots d^3 q_n}{(2\pi)^{3n}}(2\pi)^3 \delta_D\left(\sum \boldsymbol{q}_i - \boldsymbol{k}\right)$$

$$\times \begin{pmatrix} F_n(\{\boldsymbol{q}_i\}) \\ G_n(\{\boldsymbol{q}_i\}) \end{pmatrix}\delta_0(\boldsymbol{q}_1)\ldots\delta_0(\boldsymbol{q}_n). \qquad (A14)$$

The kernels F_n and G_n satisfy recurrence relations that follow straightforwardly from the equations of motion [21–23]:

$$F_n(\boldsymbol{q}_1, \ldots, \boldsymbol{q}_n) = \sum_{m=1}^{n-1} \frac{G_m(\boldsymbol{q}_1, \ldots, \boldsymbol{q}_m)}{(2n+3)(n-1)}\left[(1+2n)\right.$$

$$\times \frac{\boldsymbol{k} \cdot \boldsymbol{k}_1}{k_1^2}F_{n-m}(\boldsymbol{q}_{m+1}, \ldots, \boldsymbol{q}_n)$$

$$\left. + \frac{k^2(\boldsymbol{k}_1 \cdot \boldsymbol{k}_2)}{k_1^2 k_2^2}G_{n-m}(\boldsymbol{q}_{m+1}, \ldots, \boldsymbol{q}_n)\right],$$

$$\qquad (A15)$$

$$G_n(\boldsymbol{q}_1, \ldots, \boldsymbol{q}_n) = \sum_{m=1}^{n-1} \frac{G_m(\boldsymbol{q}_1, \ldots, \boldsymbol{q}_m)}{(2n+3)(n-1)}$$

$$\times \left[3\frac{\boldsymbol{k} \cdot \boldsymbol{k}_1}{k_1^2}F_{n-m}(\boldsymbol{q}_{m+1}, \ldots, \boldsymbol{q}_n)\right.$$

$$\left. + n\frac{k^2(\boldsymbol{k}_1 \cdot \boldsymbol{k}_2)}{k_1^2 k_2^2}G_{n-m}(\boldsymbol{q}_{m+1}, \ldots, \boldsymbol{q}_n)\right],$$
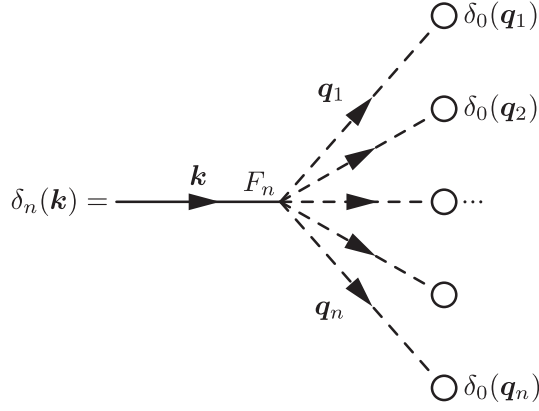
$$\qquad (A16)$$

FIG. 9.   Diagrammatic representation of the nth order contribution to $\delta(\mathbf{k})$.

where $\mathbf{k}_1 = \mathbf{q}_1 + \cdots + \mathbf{q}_m$, $\mathbf{k}_2 = \mathbf{q}_{m+1} + \cdots + \mathbf{q}_n$, $\mathbf{k} = \mathbf{k}_1 + \mathbf{k}_2$ and $F_1 = G_1 = 1$.

While the Einstein-de Sitter approximation is convenient, it is not necessary [53]. However, we have confirmed that an accurate approximation is to substitute the growth factor $D(z)$ for a,

$$\delta(\mathbf{k}; z) = \sum_{n=1}^{\infty} D^n(z)\delta_n(\mathbf{k}),$$

$$\theta(\mathbf{k}; z) = -\mathcal{H}f \sum_{n=1}^{\infty} D^n(z)\theta_n(\mathbf{k}),$$

(A17)

with the same mode-coupling integrals as above for δ_n and θ_n. The validity of this approximation is ultimately traced to the fact that the ratio Ω_m/f^2 is very nearly unity over the entire lifetime of the universe for ΛCDM cosmologies, since $f \approx \Omega_m^{0.6}$ [12].

To compute statistical observables, it is convenient to introduce diagrammatic rules for keeping track of the various terms in the perturbation series [21]. The function $\delta_n(\mathbf{k})$ [or $\theta_n(\mathbf{k})$] may be represented as in Fig. 9, where the open circles denote factors of δ_0, and the vertex denotes a momentum-conserving integral of F_n (or G_n) over intermediate wave vectors $\mathbf{q}_i$. Algebraically the nth order contribution $P^{(n)}$ is obtained by isolating all terms of order $(\delta_0)^{2n}$ from the ensemble average $\langle \delta(\mathbf{k})\delta(\mathbf{k}')\rangle$, i.e.

$$(2\pi)^3 \delta_D(\mathbf{k} + \mathbf{k}')P^{(n)}(k; z) = D^{2n}(z) \sum_{m=1}^{2n-1} \langle \delta_m(\mathbf{k})\delta_{2n-m}(\mathbf{k}')\rangle.$$

(A18)

The quantity $\langle \delta_m(\mathbf{k})\delta_{2n-m}(\mathbf{k}')\rangle$ may be represented diagrammatically by "multiplying" the diagrams for $\delta_m(\mathbf{k})$ and $\delta_{2n-m}(\mathbf{k}')$. Since the initial field δ_i (and hence δ_0) is Gaussian, ensemble averages of powers of δ_0 may be expanded in terms of the two-point function P_0 according to Wick's theorem. Then the product of the diagrams $\delta_m(\mathbf{k})$ and $\delta_{2n-m}(\mathbf{k}')$ is given by summing over all possible pairings of their open circles, where open circles are paired according to the rule

$$\text{(A19)}$$

with the additional understanding that any diagram containing a tadpole (a fragment connected to the rest of the diagram by a single edge) vanishes identically.

As an example we show in Fig. 10 how to obtain the 2nd order contribution $P^{(2,2)}(k)$. Notice that after invoking momentum conservation at vertices and translational invariance of the two-point function, only a single wave vector remains to be integrated. In general all diagrams contributing to $P^{(n)}$ contain $n - 1$ loops, requiring integration over

$n - 1$ independent wave vectors. For this reason we often classify power spectrum terms by their number of loops rather than their "order," which is a potentially ambiguous concept.

With this expansion, statistical observables may be computed straightforwardly in SPT to any fixed order. For example, the first correction to the matter power spectrum (second order in the initial power spectrum, fourth order in the initial density contrast, or one-loop in the diagrammatic

FIG. 10.   Diagrammatic prescription for computing $P^{(2,2)}(k)$. The overall factor of 2 comes from the two equivalent ways of pairing the open circles. Only the single wave vector $\mathbf{q}$ must be integrated over, the rest being determined by momentum conservation at vertices and translational invariance of the two-point function.

idiom) is given by

$$P(k) = P_L(k) + P^{(2,2)}(k) + P^{(1,3)}(k), \tag{A20}$$

where $P_L(k; z) = D^2(z)P_0(k)$ is the linear power spectrum and [22]

$$P^{(1,3)}(k) = \frac{1}{252} \frac{k^3}{4\pi^2} P_L(k) \int_0^\infty dr P_L(kr) \left[\frac{12}{r^2} - 158 + 100r^2 - 42r^4 + \frac{3}{r^2}(r^2 - 1)^3(7r^2 + 2)\ln\left|\frac{1 + r}{1 - r}\right|\right], \tag{A21a}$$

$$P^{(2,2)}(k) = \frac{1}{98} \frac{k^3}{4\pi^2} \int_0^\infty dr P_L(kr) \int_{-1}^1 dx P_L(k\sqrt{1 + r^2 - 2rx}) \frac{(3r + 7x - 10rx^2)^2}{(1 + r^2 - 2rx)^2}. \tag{A21b}$$

At low k, $P^{(2,2)}$ is positive while $P^{(1,3)}$ is negative, and there is a large degree of cancellation between them. For large k

$$P^{(2,2)}(k) \sim \tfrac{1}{4}\Sigma^2 k^2 P_L(k) \quad \text{and} \quad P^{(1,3)}(k) \sim -\tfrac{1}{2}\Sigma^2 k^2 P_L(k), \tag{A22}$$

where Σ is defined by Eq. (7), so for sufficiently large k the total second order contribution is negative.

It is also straightforward to derive expressions for the velocity power spectrum [22]

$$P_{\theta\theta}^{(1,3)}(k) = \frac{1}{84} \frac{k^3}{4\pi^2} P_L(k) \int_0^\infty dr P_L(kr) \left[\frac{12}{r^2} - 82 + 4r^2 - 6r^4 + \frac{3}{r^2}(r^2 - 1)^3(r^2 + 2)\ln\left|\frac{1 + r}{1 - r}\right|\right], \tag{A23}$$

$$P_{\theta\theta}^{(2,2)}(k) = \frac{1}{98} \frac{k^3}{4\pi^2} \int_0^\infty dr P_L(kr) \int_{-1}^1 dx P_L(k\sqrt{1 + r^2 - 2rx}) \frac{(7x - r - 6rx^2)^2}{(1 + r^2 - 2rx)^2}, \tag{A24}$$

the density-velocity cross-spectrum (e.g. [54])

$$P_{\delta\theta}^{(1,3)}(k) = \frac{1}{252} \frac{k^3}{4\pi^2} P_L(k) \int_0^\infty dr P_L(kr) \left[\frac{24}{r^2} - 202 + 56r^2 - 30r^4 + \frac{3}{r^2}(r^2 - 1)^3(5r^2 + 4)\ln\left|\frac{1 + r}{1 - r}\right|\right], \tag{A25}$$

$$P_{\delta\theta}^{(2,2)}(k) = \frac{1}{98} \frac{k^3}{4\pi^2} \int_0^\infty dr P_L(kr) \int_{-1}^1 dx P_L(k\sqrt{1 + r^2 - 2rx}) \frac{(3r + 7x - 10rx^2)(7x - r - 6rx^2)}{(1 + r^2 - 2rx)^2}, \tag{A26}$$

and the propagator

$$G(k) \simeq 1 + \frac{P^{(1,3)} + P^{(1,5)} + \cdots}{2P_L}. \tag{A27}$$

Though it is not usually considered, there is no real obstacle in going to the next order in the systematic perturbative expansion described above. For the third order (two-loop) contribution, one finds $P^{(3)}(k) = P^{(1,5)}(k) + P^{(2,4)}(k) + P^{(3,3)}(k)$ with [24]

$$P^{(1,5)}(k) = 30P_L(k) \int \frac{d^3q}{(2\pi)^3} \frac{d^3p}{(2\pi)^3} F_5^{(s)}(\boldsymbol{k}, \boldsymbol{q}, -\boldsymbol{q}, \boldsymbol{p}, -\boldsymbol{p})P_L(q)P_L(p) \tag{A28}$$

$$P^{(2,4)}(k) = 24 \int \frac{d^3q}{(2\pi)^3} \frac{d^3p}{(2\pi)^3} F_2^{(s)}(\boldsymbol{q}, \boldsymbol{k} - \boldsymbol{q})F_4^{(s)}(-\boldsymbol{q}, \boldsymbol{q} - \boldsymbol{k}, \boldsymbol{p}, -\boldsymbol{p})P_L(q)P_L(p)P_L(|\boldsymbol{k} - \boldsymbol{q}|) \tag{A29}$$

$$P^{(3,3)}(k) = \int \frac{d^3q}{(2\pi)^3} \frac{d^3p}{(2\pi)^3} [9F_3^{(s)}(\boldsymbol{q}, -\boldsymbol{q}, \boldsymbol{k})F_3^{(s)}(-\boldsymbol{k}, \boldsymbol{p}, -\boldsymbol{p})P_L(k)P_L(q)P_L(p)$$
$$+ 6F_3(\boldsymbol{q}, \boldsymbol{p}, \boldsymbol{k} - \boldsymbol{q} - \boldsymbol{p})F_3(-\boldsymbol{q}, -\boldsymbol{p}, \boldsymbol{q} + \boldsymbol{p} - \boldsymbol{k})P_L(q)P_L(p)P_L(|\boldsymbol{k} - \boldsymbol{q} - \boldsymbol{p}|)] \tag{A30}$$

and with $F_n^{(s)}$ given by Eq. (A15) symmetrized over its n arguments $\boldsymbol{q}_1, \ldots, \boldsymbol{q}_n$. Using rotational symmetry to eliminate one azimuthal integration, the resulting expressions require five-dimensional mode-coupling integrals which are best performed using Monte Carlo methods.

Expressions for higher-order contributions are not difficult to derive, but the computational costs of evaluating them quickly spiral out of control. In general the ℓ-loop contribution requires mode-coupling integrals of dimension 3ℓ ($3\ell - 1$ after rotational symmetry), making

one-loop simple, two-loop possible, and higher orders impracticable.

APPENDIX B: LAGRANGIAN PERTURBATION THEORY

The Lagrangian description of structure formation [55–57] relates the current, or Eulerian, position of a mass element, x, to its initial, or Lagrangian, position, q, through a displacement vector field: $x = q + \Psi(q)$. (Note that q is used as a position vector in the Lagrangian picture, whereas the same symbol is used as a wave vector in the Eulerian picture.) The displacements can be related to overdensities by [58]

$$
\delta(x) = \int d^3q\, \delta_D(x - q - \Psi) - 1,
$$
$$
\delta(k) = \int d^3q\, e^{-ik\cdot q}(e^{-ik\cdot\Psi(q)} - 1). \tag{B1}
$$

The displacements evolve according to

$$
\frac{d^2\Psi}{dt^2} + 2H\frac{d\Psi}{dt} = -\nabla_x\phi[q + \Psi(q)], \tag{B2}
$$

where here and only here ϕ is the gravitational potential. Analogous to Eulerian perturbation theory, standard LPT expands the displacement in powers of the linear density field with [59]

$$
\Psi^{(n)}(k) = \frac{i}{n!}\int\prod_{i=1}^{n}\left[\frac{d^3k_i}{(2\pi)^3}\right](2\pi)^3\delta_D\left(\sum_i k_i - k\right)
$$
$$
\times L^{(n)}(k_1,\ldots,k_n,k)\delta_0(k_1)\ldots\delta_0(k_n), \tag{B3}
$$

and the $L^{(n)}$ have closed form expressions in terms of dot products of wave vectors which can be generated by recurrence relations. Expanding the exponential in Eq. (B1) we obtain a perturbative series for the overdensity, $\delta = \delta^{(1)} + \delta^{(2)} + \cdots$ where, e.g.,

$$
\delta^{(2)}(k) = \frac{1}{2}\int\frac{d^3k_1 d^3k_2}{(2\pi)^3}\delta_D(k_1 + k_2 - k)\delta_0(k_1)\delta_0(k_2)
$$
$$
\times [k\cdot L^{(2)}(k_1,k_2,k) + k\cdot L^{(1)}(k_1)k\cdot L^{(1)}(k_2)] \tag{B4}
$$

is second order in the linear density field δ_0.

A similar expansion can be performed for the power spectrum, which from Eq. (B1) can be written

$$
P(k) = \int d^3q\, e^{-ik\cdot q}(\langle e^{-ik\cdot\Delta\Psi}\rangle - 1), \tag{B5}
$$

where $\Delta\Psi = \Psi(q) - \Psi(0)$ and we have used translational invariance.

Alternatively [28] suggested using the cumulant expansion theorem for the exponential in Eq. (B5) and using the binomial theorem to expand the term $(k\cdot\Delta\Psi)^N$. One obtains two types of terms: those depending on Ψ at the same point and those depending on Ψ at two different points. Owing to statistical homogeneity the first type of term is independent of position and can be factored out of the integral leaving [28]

$$
P(k) = \exp\left[-2\sum_{n=1}^{\infty}(-1)^{n-1}\langle[k\cdot\Psi(0)]^{2n}\rangle\right]
$$
$$
\times\int d^3r\, e^{ik\cdot r}\left\{\exp\left[\sum_{N=2}^{\infty}\frac{k_{i_1}\ldots k_{i_N}}{N!}B^{(N)}_{i_1\ldots i_N}(r)\right] - 1\right\}, \tag{B6}
$$

where $k_{i_1}\ldots k_{i_N}B^{(N)}_{i_1\ldots i_N}(r)$ is shorthand for the second type of term.

In a traditional perturbative calculation, one would expand this expression to a fixed order in Ψ; this approach indeed reproduces the SPT result to 2nd order. However, one might expect that the position-independent cumulant factors are more important on large scales than the position-dependent ones, suggesting that these factors should be left unexpanded in the exponential. Using well-known previous results from LPT, the first corrections to the power spectrum are then [28]

$$
P(k) = e^{-(k\Sigma)^2/2}[P_L(k) + P^{(2,2)}(k) + \tilde{P}^{(1,3)}(k)], \tag{B7}
$$

where Σ is given by Eq. (7), $P^{(2,2)}(k)$ is as in SPT [Eq. (A21b)] and

$$
\tilde{P}^{(1,3)}(k) = \frac{1}{252}\frac{k^3}{4\pi^2}P_L(k)\int_0^{\infty}dr\, P_L(kr)
$$
$$
\times\left[\frac{12}{r^2} + 10 + 100r^2 - 42r^4\right.
$$
$$
\left. + \frac{3}{r^3}(r^2 - 1)^3(7r^2 + 2)\ln\left|\frac{1+r}{1-r}\right|\right]. \tag{B8}
$$

Notice that this differs from the SPT result [Eq. (A21a)] only by the replacement $-158 \to 10$ in the brackets. If the exponential prefactor is expanded to first order in P_L, the SPT result is recovered exactly [28]. Also note that the first term $e^{-\Sigma^2 k^2/2}P_L(k)$ is identical to the tree-level RPT result in the large-k limit.

[1] D. J. Eisenstein, New Astron. Rev. **49**, 360 (2005).

[2] T. Nishimichi *et al.*, Publ. Astron. Soc. Jpn. **61**, 321 (2009).

[3] A. Taruya and T. Hiramatsu, Astrophys. J. **674**, 617 (2008).

[4] F. Bernardeau, M. Crocce, and R. Scoccimarro, Phys. Rev. D **78**, 103521 (2008).

[5] P. Valageas, Astron. Astrophys. **484**, 79 (2008).

[6] H. Guo and Y. P. Jing, Astrophys. J. **698**, 479 (2009).

[7] A. E. Evrard *et al.*, Astrophys. J. **672**, 122 (2008).

[8] K. Heitmann *et al.*, Comput. Sci. Discovery **1**, 015003 (2008).

[9] K. Heitmann, M. White, C. Wagner, S. Habib, and D. Higdon, arXiv:0812.1052.

[10] G. Hinshaw *et al.*, Astrophys. J. Suppl. Ser. **180**, 225 (2009).

[11] A. Slosar, C. Hirata, U. Seljak, S. Ho, and N. Padmanabhan, J. Cosmol. Astropart. Phys. 08 (2008) 031.

[12] F. Bernardeau, S. Colombi, E. Gaztañaga, and R. Scoccimarro, Phys. Rep. **367**, 1 (2002).

[13] M. Crocce and R. Scoccimarro, Phys. Rev. D **73**, 063519 (2006).

[14] M. Crocce and R. Scoccimarro, Phys. Rev. D **73**, 063520 (2006).

[15] S. Bharadwaj, Astrophys. J. **460**, 28 (1996).

[16] S. Bharadwaj, Astrophys. J. **472**, 1 (1996).

[17] V. L'vov and I. Procaccia, arXiv:chao-dyn/9502010.

[18] P. J. E. Peebles, *The Large-Scale Structure of the Universe* (Princeton University Press, Princeton, NJ, 1980).

[19] R. Juszkiewicz, Mon. Not. R. Astron. Soc. **197**, 931 (1981).

[20] E. T. Vishniac, Mon. Not. R. Astron. Soc. **203**, 345 (1983).

[21] M. H. Goroff, B. Grinstein, S.-J. Rey, and M. B. Wise, Astrophys. J. **311**, 6 (1986).

[22] N. Makino, M. Sasaki, and Y. Suto, Phys. Rev. D **46**, 585 (1992).

[23] B. Jain and E. Bertschinger, Astrophys. J. **431**, 495 (1994).

[24] J. N. Fry, Astrophys. J. **421**, 21 (1994).

[25] M. Crocce and R. Scoccimarro, Phys. Rev. D **77**, 023533 (2008).

[26] M. Pietroni, J. Cosmol. Astropart. Phys. 10, (2008) 036.

[27] P. Valageas, Astron. Astrophys. **465**, 725 (2007).

[28] T. Matsubara, Phys. Rev. D **77**, 063530 (2008).

[29] H. W. Wyld Jr., Ann. Phys. (N.Y.) **14**, 143 (1961).

[30] J. Lesgourgues, S. Matarrese, M. Pietroni, and A. Riotto, J. Cosmol. Astropart. Phys. 06, (2009) 017.

[31] P. McDonald, Phys. Rev. D **75**, 043514 (2007).

[32] P. Valageas, Astron. Astrophys. **379**, 8 (2001).

[33] P. Valageas, Astron. Astrophys. **382**, 412 (2002).

[34] P. Valageas, Astron. Astrophys. **421**, 23 (2004).

[35] P. Valageas (private communication).

[36] T. Matsubara, Phys. Rev. D **78**, 083519 (2008).

[37] T. Buchert, Mon. Not. R. Astron. Soc. **254**, 729 (1992).

[38] T. Buchert and J. Ehlers, Mon. Not. R. Astron. Soc. **264**, 375 (1993).

[39] T. Buchert, Mon. Not. R. Astron. Soc. **267**, 811 (1994).

[40] http://www.camb.info

[41] M. White, Astrophys. J. Suppl. Ser. **143**, 241 (2002).

[42] V. Springel, Mon. Not. R. Astron. Soc. **364**, 1105 (2005).

[43] R. W. Hockney and J. W. Eastwood, *Computer Simulation Using Particles* (Hilger, Bristol, 1988).

[44] M. White, Y.-S. Song, and W. J. Percival, arXiv: 0810.1518.

[45] D. Jeong and E. Komatsu, Astrophys. J. **651**, 619 (2006).

[46] We bin the model into the same finite-width bins as the N-body data when making the comparison to the latter.

[47] E. Sefusatti and E. Komatsu, Phys. Rev. D **76**, 083004 (2007).

[48] T. Hiramatsu and A. Taruya, Phys. Rev. D **79**, 103526 (2009).

[49] http://mwhite.berkeley.edu/Copter

[50] N. Afshordi, Phys. Rev. D **75**, 021302 (2007).

[51] W. J. Percival and M. White, arXiv:0808.0003.

[52] S. Pueblas and R. Scoccimarro, Phys. Rev. D **80**, 043504 (2009).

[53] R. Takahashi, Prog. Theor. Phys. **120**, 549 (2008).

[54] R. Scoccimarro, Phys. Rev. D **70**, 083007 (2004).

[55] T. Buchert, Astron. Astrophys. **223**, 9 (1989).

[56] F. Moutarde, J.-M. Alimi, F. R. Bouchet, R. Pellat, and A. Ramani, Astrophys. J. **382**, 377 (1991).

[57] E. Hivon, F. R. Bouchet, S. Colombi, and R. Juszkiewicz, Astron. Astrophys. **298**, 643 (1995).

[58] A. N. Taylor and A. J. S. Hamilton, Mon. Not. R. Astron. Soc. **282**, 767 (1996).

[59] F. R. Bouchet, S. Colombi, E. Hivon, and R. Juszkiewicz, Astron. Astrophys. **296**, 575 (1995).

[60] D. J. Eisenstein and W. Hu, Astrophys. J. **496**, 605 (1998).